

AN AUGMENTED BACKWARD-CORRECTED PROJECTOR SPLITTING INTEGRATOR FOR DYNAMICAL LOW-RANK TRAINING*

JONAS KUSCH [†], STEFFEN SCHOTTHÖFER [‡], AND ALEXANDRA WALTER [§]

Abstract. Layer factorization has emerged as a widely used technique for training memory-efficient neural networks. However, layer factorization methods face several challenges, particularly a lack of robustness during the training process. To overcome this limitation, dynamical low-rank training methods have been developed, utilizing robust time integration techniques for low-rank matrix differential equations. Although these approaches facilitate efficient training, they still depend on computationally intensive QR and singular value decompositions of matrices with small rank. In this work, we introduce a novel low-rank training method that reduces the number of required QR decompositions. Our approach integrates an augmentation step into a projector-splitting scheme, ensuring convergence to a locally optimal solution. We provide a rigorous theoretical analysis of the proposed method and demonstrate its effectiveness across multiple benchmarks.

Key words. Dynamical Low-Rank Training, Dynamical Low-Rank Approximation, Neural Network Training, Projector Splitting Integrator

AMS subject classifications. 68T07, 49Q12, 65L05, 65L20, 65L70

1. Introduction. Machine learning models are continually advancing in their ability to tackle complex tasks, such as segmenting organs at risk and target volumes on CT scans for radiation therapy [43, 10], providing language-based information and assistance [4], or generating images [18, 24]. Along with this growing complexity and capability, the number of parameters - including depth, width, and feature channels of artificial neural networks - has increased tremendously in recent years [1, 49]. In addition to advancements in processing units, managing these large parameter sets relies on various model compression techniques [32]. These techniques leverage the observation that models are commonly over-parameterized [14, 3, 11] which has been exploited since the 1990s [31, 17]. The most prominent compression techniques are sparsification [15, 35, 20, 25], quantization [44, 9], and layer factorization. The latter has recently gained considerable attention, especially for fine-tuning tasks

*Submitted to the editors February 05, 2025.

Funding: Alexandra Walter is funded by the Helmholtz Information & Data Science School for Health (HIDSS4Health). A 3-month research stay of AW at the Norwegian University of Life Sciences (NMBU) was funded by the Norway Exchange Program of the Helmholtz Information and Data Science Academy (HIDA).

The work of Steffen Schotthöfer is sponsored by the Applied Mathematics Program at the Office of Advanced Scientific Computing Research, U.S. Department of Energy, and performed at the Oak Ridge National Laboratory, which is managed by UT-Battelle, LLC under Contract No. DE-AC05-00OR22725 with the U.S. Department of Energy. The United States Government retains and the publisher, by accepting the article for publication, acknowledges that the United States Government retains a non-exclusive, paid-up, irrevocable, world-wide license to publish or reproduce the published form of this manuscript, or allow others to do so, for United States Government purposes. The Department of Energy will provide public access to these results of federally sponsored research in accordance with the DOE Public Access Plan (<http://energy.gov/downloads/doe-public-access-plan>).

[†]Norwegian University of Life Sciences, Ås, Norway (jonas.kusch@nmbu.no).

[‡]Computer Science and Mathematics Division, Oak Ridge National Laboratory, Oak Ridge, TN 37831 USA (schotthofers@ornl.gov).

[§]Corresponding author: Scientific Computing Center, Karlsruhe Institute of Technology (KIT), Karlsruhe, Germany; Division of Medical Physics in Radiation Oncology, German Cancer Research Center (DKFZ); Heidelberg, Germany; Heidelberg Institute of Radiation Oncology (HIRO) & National Center for Radiation Research in Oncology (NCRO), Heidelberg/Dresden, Germany (alexandra.walter@kit.edu).

[23, 41, 47, 19, 48, 33, 40], however also for pre-training [42, 26, 38, 39, 45, 48]. While some of these methods reduce network size after training, others can compress the network during training. Approaches in the latter category avoid the computationally expensive training of a full-scale network, significantly reducing both computational costs and memory requirements. While common training strategies that compress the model during training often lack guarantees of reaching a local optimum, a family of training methods based on the theory of dynamical low-rank approximation [29] overcomes this limitation, as these methods are specifically designed to satisfy local optimality conditions [38, 46, 39, 40].

In this dynamical low-rank training [38], the weights of a neural network are compressed by restricting them to the manifold of low-rank matrices. Therefore, during training, instead of storing and updating large weight matrices, only their factorized form, i.e., small, narrow matrices, are required. The strategy to efficiently and robustly train these factorized matrices is to reformulate the training process as a gradient flow and to evolve the resulting matrix ordinary differential equations through low-rank time integrators developed in the context of dynamical low-rank approximation (DLRA). DLRA, which has been established in [29], has been used for various problems in scientific computing, including quantum mechanics [16] and kinetic problems [13]. Various integrators have been proposed in the literature to solve the time evolution equations in dynamical low-rank approximation. The most frequently used integrators are projector–splitting integrators (PSI) [34, 27, 22] and basis-update & Galerkin (BUG) integrators [8, 6, 7]. In fields like quantum physics, the projector splitting integrator is widely used [16]. For a gyrokinetic model, the PSI shows greater efficiency, and improved stability for larger time steps with comparable accuracy when compared to other suitable integrators [12]. However, most research on kinetic equations and dynamical low-rank training has primarily focused on basis-update & Galerkin integrators. One primary reason for this development is that the PSI requires solving a subproblem that evolves the underlying dynamics backward in time. In dynamical low-rank training, this can increase the loss, destroying the convergence to optimal weights.

In this work, we analyze the PSI in the context of neural network training, resolving the issue of the backward-in-time subproblem by deriving a novel augmented backward-corrected version of the PSI that is shown to converge to a locally optimal point. The novel method introduces an augmentation step in the backward-corrected PSI of [2], allowing for rank-adaptivity while ensuring descent and local convergence guarantees. Moreover, the construction reduces the number of QR decompositions required in every training step from two to one.

The paper is structured as follows: After the introduction, we provide a background on low-rank neural networks and dynamical low-rank approximation in [section 2](#). In [section 3](#), we review the use of DLRA for neural network training and discuss projector–splitting time integration methods to train neural networks, emphasizing potential weaknesses. We present our modification to the PSI in [section 4](#) and provide the derivation of the robust error bound as well as local convergence properties in [section 5](#). Lastly, we compare different projector–splitting integrators used to train low-rank neural networks for the MNIST dataset and to fine-tune a vision transformer in [section 6](#).

2. Background and Notation.

2.1. Neural Network Training. An artificial feed-forward neural network $\mathcal{N}(x)$ is a recursive composition of affine and non-linear functions. Given non-linear

activation functions σ_i , a feed-forward neural network reads

$$\mathcal{N}(x) = \sigma_L(W^L a^{L-1}(x) + b^L),$$

where $a^{L-1}(x)$ is defined recursively by

$$\begin{aligned} a^0(x) &= x \in \mathbb{R}^{n_0}, \\ a^l(x) &= \sigma_l(W^l a^{l-1}(x) + b^l) \in \mathbb{R}^{n^l}, \quad l = 1, \dots, L. \end{aligned}$$

Here, $W_l \in \mathbb{R}^{n^l \times n^{l-1}}$ are called the weight matrices which are collected as $\mathcal{W} = \{W^1, \dots, W^L\} \in \mathbb{R}^p$. Moreover, $b^l \in \mathbb{R}^{n^l}$ are called bias vectors. Since this work focuses on weight matrices \mathcal{W} only, biases will be omitted in the following.

Training a neural network $\mathcal{N}(x)$ is the minimization of a cost function $\mathcal{L}(\mathcal{W}; \mathcal{N}(\mathcal{X}), \mathcal{Y})$ with respect to the weights \mathcal{W} for a given dataset $\mathcal{X} = \{x_1, \dots, x_s\}$ with the corresponding exact labels $\mathcal{Y} = \{y_1, \dots, y_s\}$. Here, $\mathcal{L}(\mathcal{W}; \mathcal{N}(\mathcal{X}), \mathcal{Y})$ denotes the evaluation of the cost function on the entire dataset \mathcal{X} . Hence, we aim to determine optimal weights \mathcal{W}_* such that

$$\mathcal{W}_* = \operatorname{argmin}_{\mathcal{W}} \mathcal{L}(\mathcal{W}; \mathcal{N}(\mathcal{X}), \mathcal{Y}).$$

For computational efficiency, the full cost function is replaced by a batch evaluation. Given the batch $\mathcal{X}_\xi \subset \mathcal{X}$ with corresponding exact labels \mathcal{Y}_ξ , where $\mathcal{X}_\xi = \{x_1^{(\xi)}, \dots, x_b^{(\xi)}\}$, $\mathcal{Y}_\xi = \{y_1^{(\xi)}, \dots, y_b^{(\xi)}\}$, and $b \ll s$, the loss function on the batch \mathcal{X}_ξ is given by

$$\ell(\mathcal{W}; \mathcal{N}(\mathcal{X}_\xi), \mathcal{Y}_\xi) := \frac{1}{b} \sum_{i=1}^b \mathcal{L}(\mathcal{W}; \mathcal{N}(x_i^{(\xi)}), y_i^{(\xi)}).$$

The elements in \mathcal{X}_ξ are then changed in each iteration of the training method to cover the entire training set \mathcal{X} after a sufficient amount of iterations. This batch evaluation introduces a stochastic influence. Since the pair $\mathcal{X}_\xi, \mathcal{Y}_\xi$ is drawn from the distribution of the training data in \mathcal{X} , the batch loss fulfills

$$\mathbb{E}_\xi[\ell(\mathcal{W}; \mathcal{N}(\mathcal{X}_\xi), \mathcal{Y}_\xi)] = \mathcal{L}(\mathcal{W}; \mathcal{N}(\mathcal{X}), \mathcal{Y}).$$

Batch evaluation naturally leads to the use of stochastic gradient descent as the optimizer. Specifically, for all weight matrices $W \in \mathcal{W}$, we apply the iterative scheme

$$W_{k+1} = W_k - h \nabla_W \ell(W_k; \mathcal{N}(\mathcal{X}_\xi), \mathcal{Y}_\xi),$$

where k is the training iteration, h the learning rate and training is initialized with W_0 . In expectation, for the stochastic gradient, we have

$$\mathbb{E}_\xi[\nabla_W \ell(W; \mathcal{N}(\mathcal{X}_\xi), \mathcal{Y}_\xi)] = \nabla_W \mathcal{L}(W; \mathcal{N}(\mathcal{X}), \mathcal{Y}).$$

In the following, we make several simplifications which do not lead to a loss of generality and serve the purpose of allowing an efficient presentation. We abbreviate $\nabla_W \ell$ as $\nabla \ell$ and omit the dependence of the gradient on the neural network and labels. Moreover, we assume a network with a single layer; that is, we replace \mathcal{W} with W inside the loss. We remark that the methodological results presented in [section 4](#) can be extended to a multi-layer network using, e.g., Proposition 1 of [\[40\]](#). Then, for a

given weight $W \in \mathbb{R}^{m \times n}$, the training dynamics of stochastic descent methods are governed by the stochastic gradient-flow

$$(2.1) \quad \dot{W}(t) = -\nabla \ell(W(t)), \quad W(t=0) = W_0,$$

where the dot denotes the time derivative. Note that the steepest-descent update corresponds to an explicit Euler time discretization of the gradient flow.

2.2. Dynamical Low-Rank Approximation. State-of-the-art neural networks are often massively over-parametrized, i.e., have by orders of magnitude more weights than training data, often expressed by high-dimensional weight matrices W . The price to pay is excessive memory and compute cost to train neural networks with stochastic gradient descent.

Dynamical Low-Rank Approximation (DLRA) has been proposed as a model order reduction technique for matrix ordinary differential equations in [29]. The goal is to efficiently determine the true solution $W(t) \in \mathbb{R}^{m \times n}$ of a differential equation such as (2.1), or, more generally, $\dot{W}(t) = \mathcal{F}(W(t))$, where \mathcal{F} is an arbitrary right-hand side. As our notation suggests, the solution $W(t)$ can be the weight matrix when choosing a single-layered neural network. To reduce computational costs and memory requirements, we aim to approximate $W(t)$ by a low-rank matrix $Y(t) \in \mathbb{R}^{m \times n}$ such that $\|W(t) - Y(t)\|$ is sufficiently small for all times t . Omitting dependency on time, a rank r approximation can then be written as $Y = USV^\top \in \mathcal{M}_r \subset \mathbb{R}^{m \times n}$, where the manifold of rank r matrices is denoted by \mathcal{M}_r . Here, $U \in \mathbb{R}^{m \times r}$, $S \in \mathbb{R}^{r \times r}$, and $V \in \mathbb{R}^{n \times r}$, where the columns of U and V are orthonormal. This reduces the number of entries from nm for the full-rank matrix W to $(m+n)r + r^2$ for its low-rank approximation Y . If the rank $r \ll \min\{m, n\}$, the memory footprint of the approximation is negligible compared to its full-rank counterpart. When evolving $Y(t)$ in time, one needs to ensure that $Y(t) \in \mathcal{M}_r$ at all times while ensuring that the distance to the full-rank solution is as small as possible. Following [29], this is achieved by solving

$$\|\dot{W}(t) - \dot{Y}(t)\| = \min \quad \text{s.t.} \quad \dot{Y}(t) \in \mathcal{T}_{Y(t)}\mathcal{M}_r,$$

where $\mathcal{T}_Z\mathcal{M}_r$ denotes the tangent space of \mathcal{M}_r at Z and $\|\cdot\|$ denotes the Frobenius norm. The evolution of Y along the tangent space ensures that Y stays within the low-rank manifold \mathcal{M}_r . Using the product rule and the factorization $Y = USV^\top$, we obtain

$$\dot{Y} = \dot{U}SV^\top + U\dot{S}V^\top + US\dot{V}^\top.$$

With this, and using the Gauge conditions $U^\top \dot{U} = 0$ and $V^\top \dot{V} = 0$, which ensure the uniqueness of the low-rank representation, evolution equations for the low-rank factors U , S , and V can be derived [29]. These equations solve the problem

$$(2.2) \quad \dot{Y}(t) = P(Y(t))\mathcal{F}(Y(t)),$$

where for $Z = USV^\top$ with U and V having orthonormal columns, $P(Z)$ is the projector onto the tangent space of \mathcal{M}_r at Z which takes the form $P(Z)G = UU^\top G - UU^\top GVV^\top + GVV^\top$ for general $G \in \mathbb{R}^{m \times n}$. A core difficulty when solving (2.2) is that the projector P has a prohibitively large Lipschitz constant [29, Lemma 4.2], that tends to infinity as the smallest singular value of S tends to zero. Geometrically speaking, the condition number of S determines the curvature of \mathcal{M}_r at Y , which leads

to a prohibitively small time step size to evolve the solution with a conventional time integration method. To address this issue, time integration schemes that are robust to this curvature have been proposed in, e.g., [34, 8, 6, 5, 7, 30]. In these schemes, the evolution of low-rank factors is restricted to flat subspaces in the low-rank manifold, namely the submanifolds

$$\begin{aligned}\mathcal{M}_K &= \{KV_0^\top \mid K \in \mathbb{R}^{m \times r}, \text{ and } V_0 \in \mathbb{R}^{n \times r} \text{ fixed}\}, \\ \mathcal{M}_S &= \{U_1SV_0^\top \mid S \in \mathbb{R}^{r \times r}, U_1 \in \mathbb{R}^{m \times r}, \text{ fixed and } V_0 \in \mathbb{R}^{n \times r} \text{ fixed}\}, \\ \mathcal{M}_L &= \{U_1L^\top \mid L \in \mathbb{R}^{n \times r}, \text{ and } U_1 \in \mathbb{R}^{m \times r} \text{ fixed}\},\end{aligned}$$

which exhibit a moderate curvature compared to \mathcal{M}_r .

3. Dynamical Low-Rank Approximation for Neural Network Training.

In standard neural network training, the full weight matrix W of size nm is updated until a critical point W_\star is approximately reached, where $\mathbb{E}[\nabla\ell(W_\star)] = 0$. As discussed previously, a key drawback of modern neural network architectures is the large size of weight matrices, which leads to high memory and computational costs during training and prediction. Low-rank training offers a popular solution for reducing network size by training factorized low-rank weights instead of their full-rank, memory-intensive analogs. To achieve this, a constraint is added to the optimization problem, requiring the solution to lie on the manifold of low-rank matrices. In this case, optimality in $\mathbb{R}^{m \times n}$ is commonly not possible. Instead, for a low-rank weight $Y \in \mathcal{M}_r$, the optimality criterion needs to be relaxed to $\mathbb{E}[P(Y_\star)\nabla\ell(Y_\star)] = 0$, where again $P(Z)$ is the projection onto the tangent space of \mathcal{M}_r at $Z \in \mathcal{M}_r$, see, e.g., [37, Theorem 3.4]. As shown in [40, Section 3], standard training methods can fail to converge to such an optimum. Instead, new training methods that follow the modified gradient flow problem

$$(3.1) \quad \dot{Y}(t) = -P(Y(t))\nabla\ell(Y(t))$$

need to be constructed. This problem resembles the projected flow of DLRA (2.2), which is highly stiff. Therefore, novel training methods that are robust to this stiffness need to be developed, following the principles of robust time integration methods for DLRA.

The goal of dynamical low-rank training (DLRT) [38] is to develop training methods that train a low-rank weight $Y = USV^\top$ by solving the projected gradient flow equation (3.1) while being robust to the curvature of the low-rank manifold. In the following, we review different integrators for DLRA and discuss their applicability for DLRT. To limit the introduction of new variables, we will recycle variable names when their meaning directly follows from the context in which they are used. Commonly, the full-rank weight is denoted as W , and low-rank approximations are denoted as $Y = USV^\top$ for different integrators.

3.1. Basis-update and Galerkin Integrator. The perhaps most frequently used class of integrators are basis-update & Galerkin (BUG) integrators [8, 6, 7]. These integrators approximate the projected gradient flow (3.1) robustly, even in the presence of small singular values, i.e., when S is ill-conditioned. In the fixed-rank BUG integrator [8], U and V are updated in parallel, followed by the update of S . Given our stochastic gradient-flow (2.1) for a single-layer neural network, the integrator evolves the factorized low-rank approximation $Y(t_0) = U_0S_0V_0^\top$ from time t_0 to $t_1 = t_0 + h$

according to

$$\begin{aligned}
(3.2a) \quad \dot{K}(t) &= -\nabla\ell(K(t)V_0^\top)V_0 && \text{with } K(t_0) = U_0S_0, \\
(3.2b) \quad \dot{L}(t) &= -\nabla\ell(U_0L(t)^\top)^\top U_0 && \text{with } L(t_0) = V_0S_0^\top, \\
(3.2c) \quad \dot{S}(t) &= -U_1^\top\nabla\ell(U_1S(t)V_1^\top)V_1 && \text{with } S(t_0) = U_1^\top U_0S_0V_0^\top V_1,
\end{aligned}$$

where the orthonormal U_1 and V_1 are determined by a QR factorization such that $K(t_1) = U_1R_1 \in \mathbb{R}^{m \times r}$ and $L(t_1) = V_1R_2 \in \mathbb{R}^{n \times r}$. The factorized solution at t_1 is then given by $Y(t_1) = U_1S_1V_1^\top$, where $S_1 = S(t_1)$. This process is repeated until a desired end time t_{end} is reached. While this integrator requires a predefined rank r as input, a rank-adaptive version, commonly called the augmented BUG integrator, has been proposed in [6]. This integrator changes rank r over time while retaining robustness and other favorable properties of the original fixed-rank integrator. A parallel BUG integrator has been proposed in [7], which updates all factors in parallel.

Due to its ability to adapt the rank along with its strong theoretical guarantees, training low-rank neural networks with DLRT has centered on BUG integrators. The augmented BUG integrator [6], in particular, has been applied to train both matrix-valued [38] and tensor-valued weights [46]. Recently, the parallel BUG integrator [7] was introduced in [40] for low-rank fine-tuning. The authors demonstrate that these integrators can compress weights significantly while nearly preserving the network's accuracy. Additionally, these training methods have been adapted for stochastic gradient flows, ensuring the method's robustness and guaranteeing the descent of the loss function [21].

3.2. Projector Splitting Integrator (PSI). Another well-known example of a robust integrator is the Projector Splitting Integrator (PSI), which has been proposed in [34]. For a single-layer neural network, the integrator evolves the factorized low-rank approximation from time t_0 to $t_1 = t_0 + h$ according to

$$\begin{aligned}
(3.3a) \quad \dot{K}(t) &= -\nabla\ell(K(t)V_0^\top)V_0 && \text{with } K(t_0) = U_0S_0, \\
(3.3b) \quad \dot{S}(t) &= U_1^\top\nabla\ell(U_1S(t)V_0^\top)V_0 && \text{with } U_1S(t_0) = K(t_1), \\
(3.3c) \quad \dot{L}(t) &= -\nabla\ell(U_1L(t)^\top)^\top U_1 && \text{with } L(t_0) = V_0S(t_1)^\top.
\end{aligned}$$

The factorized solution at t_1 is then given by $Y(t_1) = U_1S_1V_1^\top$, where $L(t_1) = V_1S_1^\top$ using QR factorization and repeated until the desired end time t_{end} . For this integrator, a robust error bound is proven by [27]. A key drawback of this integrator is that (3.3b) evolves the solution along the positive gradient direction (or, equivalently, into the reversed time direction of the gradient flow), which can lead to an increase in the loss during the S -step. We will investigate this statement further in Section 5, where we show that the loss cannot be guaranteed to descend because of the S -step for the PSI in Lemma 5.1.

3.3. Backward Correction of the PSI. Addressing the issue of moving backward in time, [2] proposed a backward Euler step to update S , thereby replacing the reversed time step in the standard PSI. This backward correction of the PSI evolves the factorized low-rank approximation from time t_0 to $t_1 = t_0 + h$ according to

$$\begin{aligned}
(3.4a) \quad \dot{K}(t) &= -\nabla\ell(K(t)V_0^\top)V_0 && \text{with } K(t_0) = U_0S_0, \\
(3.4b) \quad \bar{S}_1 &= U_1^\top U_0S_0 && \text{with } U_1R = K(t_1), \\
(3.4c) \quad \dot{L}(t) &= -\nabla\ell(U_1L(t)^\top)^\top U_1 && \text{with } L(t_0) = V_0\bar{S}_1^\top.
\end{aligned}$$

The factorized solution at t_1 is then again given by $Y(t_1) = U_1 S_1 V_1^\top$, where $L(t_1) = V_1 S_1^\top$ and repeated until t_{end} . Note that a projection has replaced the evolution equation for S ; hence, all low-rank factors are evolved forward in time.

Due to the backward Euler method's consistency, the resulting integrator is expected to retain a robust error bound. For the sake of completeness, we make this statement rigorous in Theorem 5.3. We show in Lemma 5.4 that for this backward-corrected PSI (bc-PSI), the loss cannot be guaranteed to descend either since

$$(3.5) \quad \ell(Y(t_0 + h)) \leq \ell(Y(t_0)) + c_1 \cdot \|(I - U_1 U_1^\top)Y(t_0)\| - hc_2,$$

with constants $c_1, c_2 > 0$. Note that this result is merely an upper bound and does not guarantee an increase in loss. It, however, provides the necessary understanding to design a novel method that provably fulfills loss descent and converges to a locally optimal point.

4. The Method: Augmented Backward-Corrected PSI (abc-PSI). In this section, we introduce the *augmented backward-corrected PSI (abc-PSI)* which is the main contribution of this paper. Starting from (3.4), we keep the K-step (3.4a) and adjust (3.4b) to incorporate a *rank augmentation* step, i.e.,

$$\bar{S}_1 = \widehat{U}_1^\top U_0 S_0 \quad \text{with } \widehat{U}_1 = \text{ortho}([U_0, K(t_1)]),$$

where we obtain the orthonormal, augmented basis matrix $\widehat{U}_1 \in \mathbb{R}^{n \times 2r}$ from the span of the old basis $U_0 \in \mathbb{R}^{n \times r}$ and the dynamics of the K-step at final time, $K(t_1) \in \mathbb{R}^{n \times r}$. Here, *ortho* denotes an orthonormalization process, e.g., computing a QR decomposition and returning the Q factor. Projection onto the span of \widehat{U}_1 yields the matrix of augmented coefficients $\bar{S}_1 \in \mathbb{R}^{2r \times r}$.

This basis augmentation serves two purposes. First, it is crucial to guarantee loss descent of the abc-PSI, see Theorem 5.8, since the problematic term $c_1 \cdot \|(I - U_1 U_1^\top)Y(t_0)\|^2$ of (3.5) vanishes if $\|(I - U_1 U_1^\top)Y(t_0)\|^2 = 0$. Thus, augmenting the basis U_1 to also contain the basis vectors of U_0 , resolves the issue. Second, it allows us to dynamically adjust the rank of the low-rank representation of the weight matrix in combination with a truncation criterion which we introduce at the end of this section.

The dynamics of the L-step are analogous to the non-augmented bc-PSI of (3.4). Only the initial condition $L(t_0) = V_0 S_1^\top \in \mathbb{R}^{n \times r}$ is replaced by an augmented initial condition $L(t_0) = V_0 \bar{S}_1^\top \in \mathbb{R}^{n \times 2r}$.

In summary, we write the continuous dynamics of the abc-PSI as

$$(4.1a) \quad \dot{K}(t) = -\nabla \ell(K(t) V_0^\top) V_0 \quad \text{with } K(t_0) = U_0 S_0,$$

$$(4.1b) \quad \bar{S}_1 = \widehat{U}_1^\top U_0 S_0 \quad \text{with } \widehat{U}_1 = \text{ortho}([U_0, K(t_1)]),$$

$$(4.1c) \quad \dot{L}(t) = -\nabla \ell(\widehat{U}_1 L(t)^\top)^\top \widehat{U}_1 \quad \text{with } L(t_0) = V_0 \bar{S}_1^\top.$$

Due to the augmentation step in (4.1b), the system (4.1) doubles in rank at each integration step. To maintain a feasible rank, we dynamically reduce the system's rank by truncating the least important basis vectors of $L(t_1)$ using a truncated singular value decomposition. To that end, we perform an SVD of $L(t_1) = P \Sigma Q^\top$, with $P \in \mathbb{R}^{n \times 2r}$, $\Sigma \in \mathbb{R}^{2r \times 2r}$, and $Q \in \mathbb{R}^{2r \times 2r}$. A widely used truncation criterion [38, 6] to select the rank at the next time step, denoted by r_1 , is given by

$$\sum_{i=r_1+1}^{2r} \sigma_i^2 < \vartheta,$$

where σ_i are the singular values of $\Sigma = \text{diag}(\sigma_1, \dots, \sigma_{2r})$ and ϑ is the truncation hyper-parameter, which is often formulated as a relative value, i.e., $\vartheta = \tau \|\Sigma\|$. The initial conditions K_* , and V_* for the next iteration of the method is given by

$$(4.2a) \quad K_* = \widehat{U}_1 Q_{[1, \dots, r_1]}^\top \text{diag}(\sigma_1, \dots, \sigma_{r_1}) \in \mathbb{R}^{n \times r_1},$$

$$(4.2b) \quad V_* = \widehat{P}_{[1, \dots, r_1]} \in \mathbb{R}^{n \times r_1},$$

where $Z_{[1, \dots, r_1]} \in \mathbb{R}^{m \times r_1}$ denotes taking the first r_1 columns of a matrix $Z^{m \times n}$. We remark that in total, we require one QR decomposition and one SVD per iteration of the proposed algorithm, whereas methods based on the BUG integrator, e.g. [38, 39, 46], or the parallel BUG, e.g. [40], require two QR and one SVD per iteration. This gives the proposed abc-PSI method an advantage in terms of computational cost, since QR and singular value decompositions, though performed for small matrices, are often the main bottleneck of DLRT algorithms.

4.1. Time integration of the K - and L -step ODEs. The proposed augmented backward-corrected PSI of (4.1) contains two differential equation systems in the K - and L -step. To obtain a practical algorithm, the systems need to be solved with a numerical integrator. Choosing the explicit Euler method as integrator, one obtains the gradient descent method with $\nabla_K \ell(K_0 R)$ indicating the gradient of ℓ with respect to K , evaluated at the point $K = K_0$, i.e., we have with $K_1 \approx K(t_1)$ and $L_1 \approx L(t_1)$

$$(4.3a) \quad K_1 = K_0 - h \nabla_K \ell(K_0 V_0^\top), \quad \text{with } K_0 = U_0 S_0,$$

$$(4.3b) \quad L_1 = L_0 - h \nabla_L \ell(\widehat{U}_1 L_0^\top), \quad \text{with } L_0 = V_0 S_0^\top U_0^\top \widehat{U}_1,$$

where $\widehat{U}_1 = \text{ortho}([K_0, K(t_1)])$. The updated solution reads $\widehat{Y}_1 = \widehat{U}_1 L_1^\top$. After the truncation described above, we denote the updated solution as $Y_1 = K_1 V_1^\top$. It is straightforward to show that

$$\nabla_K \ell(K_0 V_0^\top) = \nabla \ell(K_0 V_0^\top) V_0 \quad \text{and} \quad \nabla_L \ell(\widehat{U}_1 L_0^\top) = \nabla \ell(\widehat{U}_1 L_0^\top)^\top \widehat{U}_1$$

using the chain rule of differentiation. We remark that multiple gradient descent steps are compatible with the proposed method. Performing multiple gradient descent steps helps to offset the computational expense of the QR and SVD in the augmentation and truncation steps. A summary of the method is given in Algorithm 4.1. While it is designed for the DLRT of a single-layer network, this simplification is made to streamline the algorithm and can be easily extended to multi-layer networks.

5. Loss descent and convergence properties. In this section, we show that the non-augmented versions, PSI and backward-corrected PSI of subsection 3.2 and subsection 3.3 respectively, cannot guarantee loss descent. Subsequently, we demonstrate the analytical properties of the abc-PSI using stochastic gradient descent. Although all the following proofs are derived for DLRT of a single-layer network, all results can be directly transferred to multi-layer network training with Proposition 1 of [40].

For the remainder of this paper, $\langle \cdot, \cdot \rangle$ denotes the scalar product $\langle A, B \rangle = \text{tr}(A^T B) = \sum_{i,j} a_{ij} b_{ij}$, and $\|\cdot\|$ the Frobenius norm. The projection onto the space spanned by U , and V , are defined by $P_U := UU^\top$, and $P_V := VV^\top$ respectively.

Algorithm 4.1

 Augmented Backward-Corrected Projection Splitting Integration (abc-PSI)

Input: Low-rank factorization $Y_0 = K_0 V_0^\top \in \mathcal{M}_{r_0}$, initial rank r_0 , and truncation tolerance $\tau > 0$.

for $k = 0, 1, \dots$ and $t_{k+1} = t_k + h$ **do**

***K*-step:**

$$K_{k+1} \leftarrow K_k - h \nabla_K \ell(K_k V_k^\top)$$

$$\widehat{U}_{k+1, -} \leftarrow \text{QR.decomposition}([K_k \mid K_{k+1}]) \quad /* \text{Rank augmentation} */$$

***L*-step:**

$$L_k \leftarrow V_k K_k^\top \widehat{U}_{k+1}$$

$$L_{k+1} \leftarrow L_k - h \nabla_L \ell(\widehat{U}_{k+1} L_k)$$

Truncation step:

$$P, \Sigma, Q^\top \leftarrow \text{SVD}(L_{k+1}) \quad /* \text{With } \Sigma = \text{diag}(\sigma_1, \dots, \sigma_{2r_k}) */$$

Set $r_{k+1} \leftarrow r$ such that $\|\sigma_{r+1}, \dots, \sigma_{2r_k}\| \leq \tau \cdot \|\sigma_1, \dots, \sigma_{2r_k}\|$

$$K_{k+1} \leftarrow \widehat{U}_{k+1} Q_{[1, \dots, r_{k+1}]}^\top \cdot \text{diag}(\sigma_1, \dots, \sigma_{r_{k+1}})$$

$$V_{k+1} \leftarrow P_{[1, \dots, r_{k+1}]}$$

end for

5.1. Assumptions. For all following proofs, we make Assumptions [A1](#) - [A4](#) based on the decomposition of the deterministic gradient $\nabla \ell(Y)$ into a part $M(Y) \in \mathcal{T}_Y \mathcal{M}_r$ and a residual term $R(Y)$ such that $\nabla \ell(Y) = M(Y) + R(Y)$.

- (A1) The difference between the initial full-rank and the initial low-rank matrix is bounded by δ , i.e., $\|Y_0 - W_0\| \leq \delta$.
- (A2) The stochastic gradient $\nabla \ell$ is Lipschitz continuous with respect to $\|\cdot\|$ and Lipschitz constant $c_l > 0$.
- (A3) The stochastic gradient $\nabla \ell$ is bounded by a constant $B > 0$.
- (A4) The residual term $R(Y)$ is bounded by $\epsilon > 0$ for all $Y \in \mathcal{M}_r$.

5.2. Descent properties of the original PSI. A descent guarantee of the loss is a central element in proving the convergence of low-rank training methods. While such a property might hold for the original PSI, the descent cannot be proven with standard tools due to the negative *S*-step. It can be shown that the loss decreases in the *K*-step and the *L*-step, while it increases in the *S*-step. To formalize this statement and provide intuition for the dynamics of the PSI, we show the following bound, which is insufficient to prove the convergence of the algorithm.

LEMMA 5.1. (*Loss evaluation of the PSI*) Let $Y(t)$ be the solution of the PSI evolution equations of (3.3). Then, the loss is bounded by

$$\ell(Y(t_1)) \leq \ell(Y(t_0)) - \alpha_K^2 h + \alpha_S^2 h - \alpha_L^2 h$$

with

$$\begin{aligned} \alpha_K &= \min_{s \in [t_0, t_1]} \|\nabla \ell(Y_K(s)) V_0\|, & \text{where } Y_K(t) &:= K(t) V_0^\top, \\ \alpha_S &= \max_{s \in [t_0, t_1]} \|U_1^\top \nabla \ell(Y_S(s)) V_0\|, & \text{where } Y_S(t) &:= U_1 S(t) V_0^\top, \\ \alpha_L &= \min_{s \in [t_0, t_1]} \|\nabla \ell(Y_L(s))^\top U_1\|, & \text{where } Y_L(t) &:= U_1 L(t)^\top. \end{aligned}$$

Proof. Following [6] and [38], we investigate the loss decent in all three substeps of (3.3). Without loss of generality, we prove the bound on the interval $t \in [0, h]$, where $Y(0) =: Y_0 = U_0 S_0 V_0^\top$.

1. We first show that the K -step (3.3a) decreases the loss. Let $Y_K(t) := K(t) V_0^\top$. Then, with (3.3a) we have

$$\begin{aligned} \frac{d}{dt} \ell(Y_K(t)) &= \langle \nabla \ell(Y_K(t)), \dot{Y}_K(t) \rangle \\ &= \langle \nabla \ell(Y_K(t)), \dot{K}(t) V_0^\top \rangle \\ &\stackrel{(3.3a)}{=} \langle \nabla \ell(Y_K(t)), -\nabla \ell(K(t) V_0^\top) V_0 V_0^\top \rangle \\ &= - \langle \nabla \ell(Y_K(t)) V_0, \nabla \ell(K(t) V_0^\top) V_0 \rangle \\ &= - \|\nabla \ell(Y_K(t)) V_0\|^2. \end{aligned}$$

With $\alpha_K = \min_{0 \leq \tau \leq 1} \|\nabla \ell(Y_K(\tau h)) V_0\|$, we have $\frac{d}{dt} \ell(Y_K(t)) \leq -\alpha_K^2$. Taking the integral from $t_0 = 0$ to $t_1 = h$ yields, with $\int_0^h \frac{d}{dt} \ell(Y_K(t)) dt = \ell(Y_K(t_1)) - \ell(Y_0)$,

$$\ell(Y_K(t_1)) \leq \ell(Y_0) - \int_0^h \alpha_K^2 dt = \ell(Y_0) - \alpha_K^2 h.$$

2. We then show that the loss increases in the S -step (3.3b). Let $Y_S(t) := U_1 S(t) V_0^\top$. Then, with (3.3b) we know that

$$\begin{aligned} \frac{d}{dt} \ell(Y_S(t)) &= \langle \nabla \ell(Y_S(t)), \dot{Y}(t) \rangle \\ &= \langle \nabla \ell(Y_S(t)), U_1 \dot{S}(t) V_0^\top \rangle \\ &\stackrel{(3.3b)}{=} \langle U_1^\top \nabla \ell(Y_S(t)) V_0, \dot{S}(t) \rangle \\ &= \langle U_1^\top \nabla \ell(Y_S(t)) V_0, U_1^\top \nabla \ell(Y_S(t)) V_0 \rangle \\ &= \|U_1^\top \nabla \ell(Y_S(t)) V_0\|^2. \end{aligned}$$

With $\alpha_S = \max_{0 \leq \tau \leq 1} \|U_1^\top \nabla \ell(Y_S(\tau h)) V_0\|$, we have $\frac{d}{dt} \ell(Y_S(t)) \leq \alpha_S^2$. Taking the integral from $t_0 = 0$ to $t_1 = h$ yields, with $\int_0^h \frac{d}{dt} \ell(Y_S(t)) dt = \ell(Y_S(t_1)) - \ell(Y_K(t_1))$,

$$\ell(Y_S(t_1)) \leq \ell(Y_0) - h\alpha_K^2 + h\alpha_S^2.$$

3. We show that the L -step (3.3c) decreases the loss analogously to the K -step. Let $Y_L(t) := U_1 L(t)^\top$. As for the K -step we have

$$\frac{d}{dt} \ell(Y_L(t)) = - \|\nabla \ell(Y_L(t))^\top U_1\|^2.$$

With $\alpha_L = \min_{0 \leq \tau \leq 1} \|\nabla \ell(Y_L(\tau h))^\top U_1\|$, we have $\frac{d}{dt} \ell(Y_L(t)) \leq -\alpha_L^2$. Hence,

$$\ell(Y(t_1)) = \ell(Y_L(t_1)) \leq \ell(Y_0) - h\alpha_K^2 + h\alpha_S^2 - h\alpha_L^2. \quad \square$$

Remark 5.2. The derivation shows that if

$$\int_0^h \|\nabla \ell(Y_K(t))V_0\|^2 dt + \int_0^h \|\nabla \ell(Y_L(t))^\top U_1\|^2 dt \leq \int_0^h \|U_1^\top \nabla \ell(Y_S(t))V_0\|^2 dt,$$

then the loss increases over one time step.

5.3. Robust Error Bound of the Backward-Corrected PSI. The original PSI has already been shown to have a robust error bound even in the presence of small singular values [27]. Therefore, a similar robust error bound is expected to hold for its version in which one of the substeps changed to an implicit time discretization. For completeness, we present a rigorous proof of the robustness of the backward-corrected PSI of subsection 3.3. To analyze the robust error bound of the backward-corrected PSI, we first show that the deviation between the PSI and bc-PSI is sufficiently small for all steps K, S, and L and then conclude the robustness following the proof of the robust error bound of the original PSI [27, Theorem 2.1].

THEOREM 5.3. (*Robust error bound of the bc-PSI*) *Let us denote the weights at time $t_n = t_0 + nh$ following the original gradient flow (2.1) as $W(t_n)$ and the weights of the backward-corrected PSI following the evolution equations (3.4) as \bar{Y}_n . Under Assumptions 5.1, the global error is bounded by*

$$\|W(t_n) - \bar{Y}_n\| \leq c_1 h + c_2 \varepsilon + c_3 \delta,$$

where $c_{1,2,3}$ are independent of singular values of the numerical and exact solution.

Proof. In the following, let all variables overset by \sim describe variables taken from the original PSI, while all variables overset by $-$ describe variables taken from the bc-PSI. Moreover, let us denote an arbitrarily chosen time t_{n-1} as t_0 and t_n as t_1 . We start by bounding the distance of the results from the PSI and the bc-PSI in all three substeps where we assume that both integrators start with the same initial condition $Y_0 = U_0 S_0 V_0^\top$. That is, we start by investigating the local error in the following four steps.

1. The K -step of both integrators is the same. Thus, $\tilde{K}(t) = \bar{K}(t) =: K(t)$ for $t \in [t_0, t_1]$.
2. We note that for the original PSI, multiplying $K_1 = K(t_1)$ with V_0^\top and $\bar{S}(t_1)$ with U_1 and V_0^\top yields

$$(5.1) \quad K_1 V_0^\top = Y_0 - \int_{t_0}^{t_1} \nabla \ell(K(t)V_0^\top) V_0 V_0^\top dt$$

for the K -step, and

$$(5.2) \quad U_1 \tilde{S}_1 V_0^\top = K_1 V_0^\top + \int_{t_0}^{t_1} U_1 U_1^\top \nabla \ell(U_1 \tilde{S}(t)V_0^\top) V_0 V_0^\top dt$$

for the S -step. Next, we plug (5.1) into (5.2), which yields

$$(5.3) \quad \begin{aligned} U_1 \tilde{S}_1 V_0^\top &= Y_0 - \int_{t_0}^{t_1} \nabla \ell(K(t)V_0^\top) V_0 V_0^\top dt \\ &\quad + \int_{t_0}^{t_1} U_1 U_1^\top \nabla \ell(U_1 \tilde{S}(t)V_0^\top) V_0 V_0^\top dt. \end{aligned}$$

We add and subtract $\int_{t_0}^{t_1} U_1 U_1^\top \nabla \ell(K(t) V_0^\top) V_0 V_0^\top dt$ as well as define

$$\Delta := \int_{t_0}^{t_1} \nabla \ell(K(t) V_0^\top) dt - \int_{t_0}^{t_1} \nabla \ell(U_1 \tilde{S}(t) V_0^\top) dt.$$

Then, (5.3) becomes

$$(5.4) \quad \begin{aligned} U_1 \tilde{S}_1 V_0^\top &= K_0 V_0^\top - (I - U_1 U_1^\top) \int_{t_0}^{t_1} \nabla \ell(K(t) V_0^\top) dt V_0 V_0^\top \\ &\quad + U_1 U_1^\top \Delta V_0 V_0^\top. \end{aligned}$$

We note that

$$\begin{aligned} \|\Delta\| &\leq c_l \int_{t_0}^{t_1} \|K(t) V_0^\top - U_1 \tilde{S}(t) V_0^\top\| dt \\ &\leq c_l \int_{t_0}^{t_1} \|K(t_1) V_0^\top - U_1 \tilde{S}(t_0) V_0^\top\| dt \\ &\quad + c_l \int_{t_0}^{t_1} \int_{t_0}^t \|\dot{K}(s) V_0^\top + U_1 \dot{\tilde{S}}(s) V_0^\top\| ds dt \leq 2c_l B h^2. \end{aligned}$$

Multiplication of (5.4) with U_1^\top and V_0 yields

$$\tilde{S}_1 = U_1^\top K_0 + U_1^\top \Delta V_0.$$

Using Assumption A2 and recalling that $\bar{S}_1 = U_1^\top K_0$, we have

$$\|\tilde{S}_1 - \bar{S}_1\| \leq \|U_1^\top \Delta V_0\| \leq 2c_l B h^2.$$

3. With Assumption A2 and the orthogonality of the columns in V_0, U_1 , the distance of the results from the PSI and the bc-PSI after the L -step is bounded by

$$\begin{aligned} \|\tilde{L}_1 - \bar{L}_1\| &\leq \|\tilde{L}_0 - \bar{L}_0\| + \int_{t_0}^{t_1} \|(\nabla \ell(U_1 \tilde{L}(t)^\top)^\top - \nabla \ell(U_1 \bar{L}(t)^\top)^\top) U_1\| dt \\ &\leq \|V_0 (\tilde{S}_1 - \bar{S}_1)^\top\| + h c_l \|\tilde{L}_0 - \bar{L}_0\| + c_l \int_{t_0}^{t_1} \int_{t_0}^t \|\dot{\tilde{L}}(s) - \dot{\bar{L}}(s)\| ds dt \\ &\leq 2c_l B h^2 + 2c_l^2 B h^3 + c_l B h^2. \end{aligned}$$

4. Hence, we have that $\|\tilde{Y}_1 - \bar{Y}_1\| \leq 2c_l B h^2 + 2c_l^2 B h^3 + c_l B h^2$. Then, according to [27, Theorem 2.1], the local error is bounded by

$$(5.5) \quad \|W(t_1) - \bar{Y}_1\| \leq \|W(t_1) - \tilde{Y}_1\| + \|\tilde{Y}_1 - \bar{Y}_1\| \leq c_1 h^2 + c_2 h \varepsilon.$$

Concluding the proof, the result on the global error $\|W(t_n) - \bar{Y}_n\|$ follows from the Lady Windermere's fan argument [36, II.3] with error propagation via the exact flow; cf. [6, 8, 27, 28, 5]. \square

5.4. Descent properties of the backward-corrected PSI.

LEMMA 5.4. (*Loss evaluation of the bc-PSI*) Under Assumption A2 and A3, let $Y(t)$ be the solution of the backward-corrected PSI evolution equations of (3.4). Then, the loss is bounded by

$$\ell(Y(t_1)) \leq \ell(Y_0) + B\|(I - U_1 U_1^\top)Y_0\| + \frac{c_l}{2}\|(I - U_1 U_1^\top)Y_0\|^2 - h\alpha_L^2$$

with $\alpha_L = \min_{s \in [t_0, t_1]} \|\nabla \ell(Y_L(s))^\top U_1\|$.

Proof. As before, we investigate the time interval $[0, h]$. We start with the L -step, which analogously to the proof of Lemma 5.1 gives with $Y_L(0) = U_1 U_1^\top Y_0$

$$\ell(Y(t_1)) = \ell(Y_L(t_1)) \leq \ell(U_1 U_1^\top Y_0) - h\alpha_L^2.$$

Using Assumption A2 and Lemma 5.2. of [21] yields for general $Z_1, Z_2 \in \mathbb{R}^{m \times n}$

$$\ell(Z_1) \leq \ell(Z_2) - \langle \nabla \ell(Z_2), Z_1 - Z_2 \rangle + \frac{c_l}{2}\|Z_1 - Z_2\|^2.$$

Then, using the above inequality with $Z_1 = U_1 U_1^\top Y_0$ and $Z_2 = Y_0$ as well as the Cauchy-Schwartz inequality and boundedness of $\nabla \ell$ yields

$$\begin{aligned} \ell(Y(t_1)) &\leq \ell(Y_0) + \langle \nabla \ell(Y_0), (I - U_1 U_1^\top)Y_0 \rangle + \frac{c_l}{2}\|(I - U_1 U_1^\top)Y_0\|^2 - h\alpha_L^2 \\ &\leq \ell(Y_0) + B\|(I - U_1 U_1^\top)Y_0\| + \frac{c_l}{2}\|(I - U_1 U_1^\top)Y_0\|^2 - h\alpha_L^2. \quad \square \end{aligned}$$

While this result does not immediately show a decrease or increase in the loss, it directly shows how to adapt the method to guarantee descent. The term that can potentially increase the loss (or at least render our analytic result impractical) is $\|(I - U_1 U_1^\top)Y_0\|^2$.

5.5. Robustness of the abc-PSI. The previous derivations have shown that while the bc-PSI has a robust error bound, showing loss descent remains difficult. Loss-descent is, however, a key ingredient in proving convergence to a local low-rank optimum. In this section, we show that the abc-PSI does not suffer from this problem. Throughout the following proofs we denote the solution of the abc-PSI before truncation as $\hat{Y}_n = \hat{U}_n L(t_n)^\top$ and after truncation as $Y_n = U_n S_n V_n^\top$ where $\|\hat{Y}_n - Y_n\| \leq \vartheta$. As in the previous sections, we investigate the time interval $[t_0, t_1]$ for ease of presentation. Moreover, we use several properties of the projector $P_{\hat{U}_{k+1}} = \hat{U}_{k+1} \hat{U}_{k+1}^\top$ which we state in the following.

Remark 5.5. Using the augmented basis \hat{U}_{k+1} yields

$$(5.6a) \quad P_{\hat{U}_{k+1}} \hat{U}_{k+1} = \hat{U}_{k+1} \hat{U}_{k+1}^\top \hat{U}_{k+1} = \hat{U}_{k+1},$$

$$(5.6b) \quad P_{\hat{U}_{k+1}} U_k = \hat{U}_{k+1} \hat{U}_{k+1}^\top U_k = U_k.$$

Thus, it holds that

$$(5.7) \quad (I - P_{\hat{U}_{k+1}}) \hat{U}_{k+1} = 0.$$

Special applications of (5.7) are $(P_{\widehat{U}_{k+1}} - I)K = 0$ and $(P_{\widehat{U}_{k+1}} - I)Y = 0$, for $K = U_k S_k$ and $Y = U_k S_k V_k^\top$. Note that because \widehat{V}_{k+1} does not necessarily contain the basis vectors V_k , these equations do not hold for $P_{\widehat{V}_{k+1}}$. I.e.,

$$0 = \left(I - P_{\widehat{V}_{k+1}}\right) L(t_{k+1}) \neq \left(I - P_{\widehat{V}_{k+1}}\right) L(t_k).$$

Note that the following results, namely the robust error bound, loss descent, and convergence of the augmented backward-corrected PSI, are shown for the discrete Algorithm 4.1. These properties are not satisfied by the PSI and bc-PSI.

THEOREM 5.6. (*Robust error bound of the abc-PSI*) *Let $Y(t_n)$ denote the solution of (4.1) when using the stochastic gradient, and $W(t_n)$ denote the solution of the full-rank gradient flow (2.1) at time t_n . Under Assumptions 5.1, the global error is bounded by*

$$\|Y(t_n) - W(t_n)\| \leq \epsilon + c_1 h + c_2 \delta + \frac{\vartheta}{h},$$

where $c_{1,2}$ are independent of singular values in the exact and numerical solutions.

Proof. To bound the distance between the low-rank solution $Y(t)$ and the full-rank solution $W(t)$ after one time step from t_0 to $t_1 = t_0 + h$ when starting at the same initial condition, i.e., $W(t_0) = Y(t_0)$, we get

$$\begin{aligned} \|\widehat{Y}_1 - W(t_1)\| &= \|\widehat{U}_1 L(t_1)^\top - W(t_1)\| \\ &= \|\widehat{U}_1 L(t_0)^\top + \int_{t_0}^{t_1} \widehat{U}_1 \dot{L}(t)^\top dt - W(t_0) - \int_{t_0}^{t_1} \dot{W}(t) dt\| \\ (5.8) \quad &\leq \int_{t_0}^{t_1} \|\widehat{U}_1 \dot{L}(t)^\top - \dot{W}(t)\| dt. \end{aligned}$$

Note that we used $\widehat{U}_1 L_0^\top = W(t_0)$. Plugging in $\dot{L}(t)^\top$ from (4.1c) into (5.8) yields

$$\|\widehat{Y}_1 - W(t_1)\| \leq \int_{t_0}^{t_1} \|\widehat{U}_1 \widehat{U}_1^\top \nabla \ell(\widehat{U}_1 L(t)^\top) - \nabla \ell(W(t))\| dt.$$

With zero completion, the orthogonality of the columns of \widehat{U}_1 , and Assumption A2, we get

$$\begin{aligned} \|\widehat{Y}_1 - W(t_1)\| &\leq \int_{t_0}^{t_1} \|\widehat{U}_1 \widehat{U}_1^\top \nabla \ell(\widehat{U}_1 L(t)^\top) - \widehat{U}_1 \widehat{U}_1^\top \nabla \ell(Y_0)\| dt \\ &\quad + \int_{t_0}^{t_1} \|\widehat{U}_1 \widehat{U}_1^\top \nabla \ell(Y_0) - \nabla \ell(W(t))\| dt \\ &\leq \int_{t_0}^{t_1} \|\nabla \ell(\widehat{U}_1 L(t)^\top) - \nabla \ell(Y_0)\| dt \\ &\quad + \int_{t_0}^{t_1} \|\widehat{U}_1 \widehat{U}_1^\top \nabla \ell(Y_0) - \nabla \ell(W(t))\| dt \\ (5.9) \quad &\leq c_l \int_{t_0}^{t_1} \|\widehat{U}_1 L(t)^\top - Y_0\| dt + \int_{t_0}^{t_1} \|\widehat{U}_1 \widehat{U}_1^\top \nabla \ell(Y_0) - \nabla \ell(W(t))\| dt. \end{aligned}$$

Using $L(t)^\top = L_0^\top - \int_{s_0}^t \widehat{U}_1^\top \nabla \ell(\widehat{U}_1 L(s)) ds$ and $\widehat{U}_1 L_0^\top = Y_0$, yields

$$\begin{aligned} \int_{t_0}^{t_1} \|\widehat{U}_1 L(t)^\top - Y_0\| dt &= \int_{t_0}^{t_1} \|\widehat{U}_1 L_0^\top - \widehat{U}_1 \int_{s_0}^t \widehat{U}_1^\top \nabla \ell(\widehat{U}_1 L(s)) ds - Y_0\| dt \\ &\leq \int_{t_0}^{t_1} \int_{s_0}^s \|\nabla \ell(\widehat{U}_1 L(s))\| ds dt. \end{aligned}$$

Then, with Assumption A3, stating that $\|\nabla \ell\| \leq B$

$$(5.10) \quad c_l \int_{t_0}^{t_1} \int_{s_0}^s \|\nabla \ell(\widehat{U}_1 L(s))\| ds dt \leq c_l \int_{t_0}^{t_1} \int_{t_0}^s B ds dt \leq c_l B h^2.$$

Moreover, the second term in (5.9) can be bounded by

$$\begin{aligned} \|\widehat{U}_1 \widehat{U}_1^\top \nabla \ell(Y_0) - \nabla \ell(W(t))\| &\leq \|\widehat{U}_1 \widehat{U}_1^\top \nabla \ell(Y_0) - \nabla \ell(Y_0)\| + \|\nabla \ell(Y_0) - \nabla \ell(W(t))\| \\ &\leq \|\widehat{U}_1 \widehat{U}_1^\top \nabla \ell(Y_0) - \nabla \ell(Y_0)\| + c_l \|Y_0 - W(t)\|. \end{aligned}$$

With Taylor-Expansion we have $\|Y_0 - W(t)\| \leq B h$. Then, using this and (5.10), the inequality (5.9) becomes

$$\|\widehat{Y}_1 - W(t_1)\| \leq \int_{t_0}^{t_1} \|\widehat{U}_1 \widehat{U}_1^\top \nabla \ell(Y_0) - \nabla \ell(Y_0)\| dt + 2c_l B h^2.$$

Using $\nabla \ell(Y) = M(Y) + R(Y)$ yields

$$\begin{aligned} \|\widehat{Y}_1 - W(t_1)\| &\leq h \|\widehat{U}_1 \widehat{U}_1^\top \nabla \ell(Y_0) - \nabla \ell(Y_0)\| + 2c_l B h^2 \\ &\leq h \|(\widehat{U}_1 \widehat{U}_1^\top - I)M(Y_0)\| + h \|(\widehat{U}_1 \widehat{U}_1^\top - I)R(Y_0)\| + 2c_l B h^2. \end{aligned}$$

With $M(Y_0) = P(Y_0) \nabla \ell(Y_0) = U_0 U_0^\top \nabla \ell(Y_0) - U_0 U_0^\top \nabla \ell(Y_0) V_0 V_0^\top + \nabla \ell(Y_0) V_0 V_0^\top$ and $(\widehat{U}_1 \widehat{U}_1^\top - I)U_0 = 0$, we get

$$(\widehat{U}_1 \widehat{U}_1^\top - I)M(Y_0) = (\widehat{U}_1 \widehat{U}_1^\top - I) \nabla \ell(Y_0) V_0 V_0^\top.$$

Using that $(\widehat{U}_1 \widehat{U}_1^\top - I)K(t_1) = 0$ and $(\widehat{U}_1 \widehat{U}_1^\top - I)Y_0 = 0$, since $K(t_1)$ and Y_0 are spanned by \widehat{U}_1 this yields

$$\begin{aligned} \|\widehat{Y}_1 - W(t_1)\| &\leq h \|(\widehat{U}_1 \widehat{U}_1^\top - I) \nabla \ell(Y_0) V_0 V_0^\top\| + h \epsilon + 2c_l B h^2 \\ &= h \left\| (\widehat{U}_1 \widehat{U}_1^\top - I) \left(\nabla \ell(Y_0) V_0 V_0^\top + \frac{1}{h} (K(t_1) V_0^\top - Y_0) \right) \right\| \\ (5.11) \quad &+ h \epsilon + 2c_l B h^2, \end{aligned}$$

Lastly, we bound the norm on the right-hand side. Let us note that

$$\begin{aligned} K(t_1) V_0^\top - Y_0 &= - \int_{t_0}^{t_1} \nabla \ell(K(t) V_0^\top) V_0 V_0^\top dt \\ &= - h \nabla \ell(Y_0^\top) V_0 V_0^\top - \int_{t_0}^{t_1} (\nabla \ell(K(t) V_0^\top) - \nabla \ell(Y_0)) V_0 V_0^\top dt. \end{aligned}$$

Together with the orthonormality of $(\widehat{U}_1 \widehat{U}_1^\top - I)$, the norm in (5.11) is bounded by

$$\begin{aligned} \left\| \nabla \ell(Y_0) V_0 V_0^\top + \frac{1}{h} (K(t_1) V_0^\top - Y_0) \right\| &\leq \frac{1}{h} \int_{t_0}^{t_1} \|\nabla \ell(K(t) V_0^\top) - \nabla \ell(Y_0)\| dt \\ &\leq \frac{c_l}{h} \int_{t_0}^{t_1} \|K(t) V_0^\top - Y_0\| dt \\ &\leq \frac{c_l}{h} \int_{t_0}^{t_1} \int_{t_0}^s \|\dot{K}(s) V_0^\top\| ds dt. \end{aligned}$$

Hence, since $\|\dot{K}(s) V_0^\top\| \leq B$, the above term is bounded by $c_l B h$. Plugging this into (5.11) gives

$$(5.12) \quad \|\widehat{Y}_1 - W(t_1)\| \leq c_l B h^2 + h\epsilon + 2c_l B h^2.$$

Hence, after truncation, the local error is bounded by

$$\|Y_1 - W(t_1)\| \leq \|\widehat{Y}_1 - W(t_1)\| + \|\widehat{Y}_1 - Y_1\| \leq h\epsilon + 3c_l B h^2 + \frac{\vartheta}{h}.$$

Concluding the proof, the result on the global error $\|\widehat{Y}_1 - W(t_1)\|$ follows from applying the standard Lady Windermere's fan argument [36, II.3] with error propagation via the exact flow; cf. [6, 8, 27, 28, 5]. \square

5.6. Discrete Case: Upper Bound of the Loss Function using SGD. In the following, we restate Lemma 5.2. of [21]. This lemma holds for the stochastic as well as the deterministic gradient.

LEMMA 5.7. *Under Assumption A2, for any $Z_1, Z_2 \in \mathbb{R}^{m \times n}$ it holds that*

$$\ell(Z_1) \leq \ell(Z_2) - \langle \nabla \ell(Z_2), Z_1 - Z_2 \rangle + \frac{c_l}{2} \|Z_1 - Z_2\|^2.$$

The proof can be found in appendix A. With this, we show loss descent for sufficiently small learning rates $h \leq \frac{2}{c_l}$.

THEOREM 5.8. *(Loss descent of the abc-PSI) Under Assumption A2, the loss of the low-rank solution Y calculated with the stochastic augmented backward-corrected PSI as in (3.4) and Algorithm 4.1 using the stochastic gradient is*

$$(5.13) \quad \ell(\widehat{Y}_1) \leq \ell(Y_0) - \left(1 - \frac{hc_l}{2}\right) h \|P_{\widehat{U}_1} \nabla \ell(Y_0)\|^2.$$

Proof. We have $\widehat{Y}_1 = \widehat{U}_1 L_1^\top$, where

$$L_1^\top = L_0^\top - h \widehat{U}_1^\top \nabla \ell(\widehat{U}_1 L_0^\top).$$

Multiplying both sides with \widehat{U}_1 , yields

$$(5.14) \quad \widehat{U}_1 L_1^\top = \widehat{U}_1 L_0^\top - h \widehat{U}_1 \widehat{U}_1^\top \nabla \ell(\widehat{U}_1 L_0^\top).$$

Then, using $\widehat{Y}_1 = \widehat{U}_1 L_1^\top$, $Y_0 = \widehat{U}_1 L_0^\top$, and $P_{\widehat{U}_1} = \widehat{U}_1 \widehat{U}_1^\top$, (5.14) becomes

$$\widehat{Y}_1 = Y_0 - h P_{\widehat{U}_1} \nabla \ell(Y_0).$$

With this and Lemma 5.7, using $Z_1 = \widehat{Y}_1$ and $Z_2 = Y_0$,

$$\begin{aligned}
\ell(\widehat{Y}_1) - \ell(Y_0) &= \ell(Y_0 - hP_{\widehat{U}_1} \nabla \ell(Y_0)) - \ell(Y_0) \\
&\leq \ell(Y_0) + \langle \nabla \ell(Y_0), Y_0 - hP_{\widehat{U}_1} \nabla \ell(Y_0) - Y_0 \rangle \\
&\quad + \frac{c_l}{2} \|Y_0 - hP_{\widehat{U}_1} \nabla \ell(Y_0) - Y_0\|^2 - \ell(Y_0) \\
&= -h \langle \nabla \ell(Y_0), P_{\widehat{U}_1} \nabla \ell(Y_0) \rangle + \frac{h^2 c_l}{2} \|P_{\widehat{U}_1} \nabla \ell(Y_0)\|^2 \\
&= -h \| \widehat{P}_{\widehat{U}_1} \nabla \ell(Y_0) \|^2 + \frac{h^2 c_l}{2} \|P_{\widehat{U}_1} \nabla \ell(Y_0)\|^2. \quad \square
\end{aligned}$$

5.7. Convergence of the abc-PSI. Given the previous discussion, we can now conclude that Algorithm 4.1 converges to weights that satisfy the local optimality criterion for optimization on manifolds, see, e.g., [37, Theorem 3.4]. In the following, we assume that the learning rate can vary with respect to the iteration index, denoted by h_t . Under the Robbins-Monro conditions, we proceed to prove convergence.

THEOREM 5.9. *(Convergence of the abc-PSI) Under Assumption A2, A3, let $\ell \geq 0$ and Y_t for $t \in \mathbb{N}$ be the solutions obtained from Algorithm 4.1. Let the learning rate sequence $(h_t)_{t \in \mathbb{N}}$ satisfy the Robbins-Monro conditions*

$$\sum_{t=1}^{\infty} h_t = +\infty, \quad \sum_{t=1}^{\infty} h_t^2 < +\infty,$$

and let $\sum_{t=1}^T \mathbb{E}[\|Y_t - \widehat{Y}_t\|] \leq D < \infty$, i.e., for sufficiently large t , the rank stabilizes. Then, algorithm 4.1 using the stochastic gradient $\nabla \ell$ converges to locally optimal weights, i.e.,

$$\liminf_{T \rightarrow \infty} \mathbb{E}[\|P(Y_T) \nabla \ell(Y_T)\|^2] = 0,$$

with expected values taken over all ξ_t .

Proof. The proof adapts the proofs of [21] and [40] for the proposed integrator. For a general iteration step t , we have with (5.13)

$$\ell(\widehat{Y}_t) \leq \ell(Y_{t-1}) - \left(1 - \frac{h_t c_l}{2}\right) h_t \|\widehat{U}_t \widehat{U}_t^\top \nabla \ell(Y_{t-1})\|^2.$$

Taking the expected value over ξ_1, \dots, ξ_T and denoting the corresponding expected value as $\mathbb{E}[\cdot]$ yields

$$\begin{aligned}
\mathbb{E}[\ell(Y_t)] - \mathbb{E}[\ell(Y_{t-1})] &\leq -h_t \mathbb{E}[\|\widehat{U}_t \widehat{U}_t^\top \nabla \ell(Y_{t-1})\|^2] + \frac{c_l h_t^2}{2} \mathbb{E}[\|\widehat{U}_t \widehat{U}_t^\top \nabla \ell(Y_{t-1})\|^2] \\
&\quad + c_l \mathbb{E}[\|Y_t - \widehat{Y}_t\|] \\
&= -h_t \left(1 - \frac{c_l h_t}{2}\right) \mathbb{E}[\|\widehat{U}_t \widehat{U}_t^\top \nabla \ell(Y_{t-1})\|^2] + c_l \mathbb{E}[\|Y_t - \widehat{Y}_t\|].
\end{aligned}$$

Summing over $t = 1, \dots, T$ and using the telescoping sum on the left-hand side then yields

$$\begin{aligned}
-\ell(Y_0) \leq \mathbb{E}[\ell(Y_T)] - \ell(Y_0) &\leq -\sum_{t=1}^T h_t \left(1 - \frac{c_l h_t}{2}\right) \mathbb{E}[\|\widehat{U}_t \widehat{U}_t^\top \nabla \ell(Y_{t-1})\|^2] \\
&\quad + c_l \sum_{t=1}^T \mathbb{E}[\|Y_t - \widehat{Y}_t\|].
\end{aligned}$$

With $\sum_{t=1}^T \mathbb{E}[\|Y_t - \hat{Y}_t\|] \leq D$ we can rearrange the above inequality as

$$(5.15) \quad \begin{aligned} \sum_{t=1}^T h_t \left(1 - \frac{c_l h_t}{2}\right) \mathbb{E}[\|\hat{U}_t \hat{U}_t^\top \nabla \ell(Y_{t-1})\|^2] &\leq \ell(Y_0) + c_l \sum_{t=1}^T \mathbb{E}[\|Y_t - \hat{Y}_t\|] \\ &\leq \ell(Y_0) + c_l D. \end{aligned}$$

Note that with

$$\begin{aligned} \hat{U}_t \hat{U}_t^\top (I - P(Y_{t-1})) \nabla \ell(Y_{t-1}) &= \hat{U}_t \hat{U}_t^\top (\nabla \ell(Y_{t-1}) - U_{t-1} U_{t-1}^\top \nabla \ell(Y_{t-1})) \\ &\quad + (U_{t-1} U_{t-1}^\top - I) \nabla \ell(Y_{t-1}) V_{t-1} V_{t-1}^\top \\ &= \hat{U}_t \hat{U}_t^\top (I - U_{t-1} U_{t-1}^\top) \nabla \ell(Y_{t-1}) (I - V_{t-1} V_{t-1}^\top) = 0 \end{aligned}$$

and $\hat{U}_t \hat{U}_t^\top P(Y_{t-1}) \nabla \ell(Y_{t-1}) = P(Y_{t-1}) \nabla \ell(Y_{t-1})$ we have

$$\begin{aligned} \hat{U}_t \hat{U}_t^\top \nabla \ell(Y_{t-1}) &= \hat{U}_t \hat{U}_t^\top P(Y_{t-1}) \nabla \ell(Y_{t-1}) + \hat{U}_t \hat{U}_t^\top (I - P(Y_{t-1})) \nabla \ell(Y_{t-1}) \\ &= P(Y_{t-1}) \nabla \ell(Y_{t-1}). \end{aligned}$$

Hence, (5.15) becomes

$$\sum_{t=1}^T h_t \left(1 - \frac{c_l h_t}{2}\right) \mathbb{E}[\|P(Y_{t-1}) \nabla \ell(Y_{t-1})\|^2] \leq \ell(Y_0) + c_l D.$$

Using Assumption A3, i.e., $\|P(Y_{t-1}) \nabla \ell(Y_{t-1})\| \leq B$, when $T \rightarrow \infty$, the right-hand side remains bounded, implying that

$$\liminf_{T \rightarrow \infty} \mathbb{E}[\|P(Y_T) \nabla \ell(Y_T)\|^2] = 0. \quad \square$$

6. Numerical Experiments. The performance of the DLRT Algorithm 4.1 is demonstrated training artificial neural network on the MNIST dataset and fine-tuning a vision transformer pre-trained on ImageNet. The implementation, available in PyTorch ([GitHub repository](#)), was executed on a computer system equipped with an AMD Ryzen™ 9 3900X Processor, 128 GB RAM, and an NVIDIA GeForce RTX 3090 GPU with 24 GB VRAM. The software environment included Python 3.11.7, PyTorch 2.2.0, and CUDA 11.8.

6.1. MNIST. For each experiment, five neural networks with the following architecture were trained: an input layer with 784 nodes, four hidden layers with 500 nodes each, and an output layer with 10 nodes. First, five fully connected (dense) networks were trained as a baseline. A learning rate of $h = 0.00001$ was used to avoid instability during training. The average test accuracy for the five dense networks is 94.54 ± 0.16 .

The experimental setup included the three variations of the PSI method: (a) the original PSI (subsection 3.2), (b) the backward-corrected PSI (subsection 3.3), and (c) the augmented backward-corrected PSI (section 4) outlined in Algorithm 4.1. Each setup was tested using learning rates of 0.01 and 0.001. Fixed ranks for setups (a) and (b) were determined based on results from experiment (c), which employed truncation tolerances of $\tau \in \{0.005, 0.01, 0.02, 0.05, 0.1, 0.2\}$.

The average test accuracies of each setup along with the number of parameters computed over five models, are summarized in Table 1 and Table 2. Table 1 shows

TABLE 1

Mean test accuracy (acc.) with standard deviation of five training runs using original PSI (PSI), backward-corrected PSI (abc-PSI), and augmented backward-corrected PSI (abc-PSI) on the MNIST data set using learning rate 0.01 and different tolerances, and ranks, respectively. The number of parameters is denoted in Millions, abbreviated by "M". It is apparent that the bc-PSI and PSI fails to train for a wide range of τ , whereas the abc-PSI not only trains successfully for all τ , but also outperforms PSI and bc-PSI in lower compression regimes.

Tol [τ]	abc-PSI (ours)		# Params	PSI		# Params	bc-PSI	
	# Params	Acc [%]		Acc [%]	Acc [%]			
0.200	0.04M	95.222 \pm 0.336	0.04M	95.710 \pm 0.132	0.04M	83.964 \pm 21.789		
0.150	0.05M	95.672 \pm 0.627	0.05M	96.206 \pm 0.200	0.05M	-		
0.100	0.07M	96.310 \pm 0.365	0.07M	96.472 \pm 0.100	0.07M	-		
0.050	0.09M	96.646 \pm 0.061	0.09M	96.648 \pm 0.068	0.09M	-		
0.020	0.11M	96.894 \pm 0.158	0.11M	96.650 \pm 0.171	0.11M	-		
0.010	0.12M	97.222 \pm 0.119	0.12M	96.588 \pm 0.062	0.12M	89.350 \pm 10.366		
0.005	0.16M	97.422 \pm 0.862	0.16M	-	0.16M	90.416 \pm 9.760		

TABLE 2

Mean test accuracy (acc.) with standard deviation of five training runs using original PSI (PSI), backward-corrected PSI (abc-PSI), and augmented backward-corrected PSI (abc-PSI) on the MNIST data set using learning rate 0.001 and different tolerances, and ranks, respectively. The number of parameters is denoted in Millions, abbreviated by "M". With a smaller learning rate 0.001, PSI and bc-PSI are able to train the network, however the abc-PSI achieves the highest validation accuracy values.

Tol [τ]	abc-PSI (ours)		# Params	PSI		# Params	bc-PSI	
	# Params	Acc [%]		Acc [%]	Acc [%]			
0.200	0.04M	90.650 \pm 0.378	0.04M	92.910 \pm 0.381	0.04M	93.116 \pm 0.626		
0.150	0.05M	92.006 \pm 0.549	0.05M	93.778 \pm 0.424	0.05M	93.584 \pm 0.512		
0.100	0.06M	93.080 \pm 0.217	0.06M	94.102 \pm 0.206	0.06M	93.870 \pm 0.388		
0.050	0.07M	93.936 \pm 0.271	0.07M	94.506 \pm 0.295	0.07M	94.864 \pm 0.358		
0.020	0.08M	94.300 \pm 0.121	0.08M	94.552 \pm 0.153	0.08M	94.826 \pm 0.430		
0.010	0.08M	94.556 \pm 0.204	0.08M	94.760 \pm 0.137	0.08M	95.136 \pm 0.598		
0.0005	0.12M	95.938 \pm 0.121	0.11M	95.060 \pm 0.277	0.11M	95.400 \pm 0.292		
0.0003	0.14M	96.664 \pm 0.223	0.15M	94.442 \pm 0.160	0.15M	95.654 \pm 0.304		
0.0002	0.17M	96.936 \pm 0.115	0.17M	95.950 \pm 0.280	0.17M	94.242 \pm 0.439		

the results for training runs with a learning rate of 0.01 and Table 2 results with a learning rate of 0.001. For learning rate 0.01, the original PSI encountered training failures for one model with rank 28 and all five models with rank 33. Experiments using the backward-corrected PSI with the same learning rate exhibited instability, with 15 out of 35 models failing in total. For the augmented backward-corrected PSI at a learning rate of 0.01, one out of five models failed to train for tolerances of 0.02, 0.15, and 0.2. For configurations in which only one out of five models failed, an additional model was trained to ensure representative comparisons. Notably, no training failures occurred during these new training runs. Also no failures occurred for any setup using a learning rate of 0.001.

To measure the parameter reduction achieved through the dynamic low-rank approximation method, the compression rate was calculated as

$$\text{compression rate} = \left(1 - \frac{\sum_l (i_l + o_l) \cdot r_l}{\sum_l i_l \cdot o_l} \right) \cdot 100$$

where i_l and o_l denote the input and output dimensions of layer l , respectively, and r_l representing its rank. Figure 1 compares the compression rate with the mean

test accuracy across all setups, excluding bc-PSI with a learning rate of 0.01 due to frequent training failures. The figure reveals that setups trained with a learning rate of 0.01 generally outperform those with smaller learning rates. Furthermore, accuracy improves as compression decreases in all configurations except for the original PSI method. This discrepancy could be attributed to unstable training dynamics. I.e., for the original PSI, no training was successful at low compression rates, as all models failed when using a rank of 33. For compression rates exceeding 91%, the original PSI with a learning rate of 0.01 outperforms all other methods, achieving its peak accuracy of 96.65% with a rank of 25. However, this method becomes unstable when dealing with larger parameter counts, causing most training runs to fail. Notably, only models trained with the abc-PSI achieve accuracies above 97% while maintaining substantial compression above 86%. Thus, the best performance for the MNIST dataset was observed in the setup employing abc-PSI with a tolerance of 0.005 and a learning rate of 0.01. This configuration achieved the highest average test accuracy (97.42%) across five models, as well as the highest accuracy for a single model (97.65%).

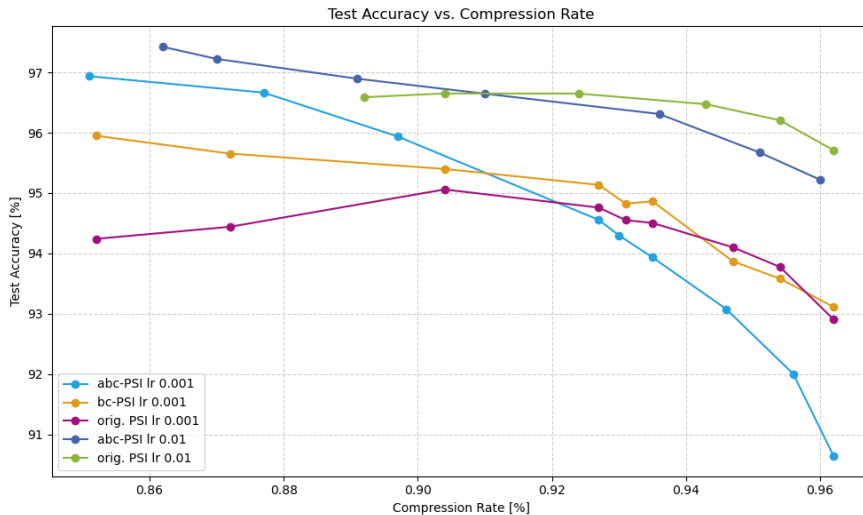


FIG. 1. Mean test accuracy of all experimental setups (PSI, bc-PSI, abc-PSI) trained on the MNIST dataset, plotted against their compression rates using learning rates of 0.01 and 0.001. Compression rates correspond to different rank selections (for fixed-rank settings) or varying tolerances (for rank-adaptive settings). Training with a learning rate of 0.01 was unstable for all backward-corrected PSI trainings and original PSI models with ranks $r > 28$, frequently leading to failed trainings; these cases are excluded from the graphic.

6.2. Vision Transformer fine-tuning for image classification. We consider a pre-trained Vit-base-patch16-224 vision transformer and use the proposed augmented backward-corrected PSI to fine-tune the vision transformer on the smaller dataset. Fine-tuning means in this context, that an additive correction Y is introduced for each pre-trained weight matrix W_{pre} of the neural network model. That is, each linear layer with input x of the model, e.g. $Wx + b$, becomes $Wx + Yx + b$. The correction Y is parametrized as USV^T , thus the abc-PSI can readily be applied to fine-tune the pre-trained base model.

We compare the proposed method to well known fine-tuning methods:

1. Low-Rank Adaptation (LoRA) [23], which parametrizes $Y = AB^T$, where

TABLE 3

Vit-base-patch16-224 fine-tuning on Cifar10, and Cifar100. We compare the number of parameters and the networks’ accuracies of the abc-PSI to LoRA, AdaLoRA and GeoLoRA reporting the median of 5 runs. The number of parameters is denoted in Millions, abbreviated by "M". The abc-PSI achieves slightly higher validation accuracy for Cifar10 with less parameters and for Cifar100 achieves similar accuracy with slightly lower number of trainable parameters.

Method	Cifar 10 [%]		Cifar 100 [%]	
	# Params	Acc [%]	# Params	Acc [%]
LoRA	0.47M (r=3)	98.47	0.47M (r=3)	91.47
AdaLoRA	0.47M	98.51	0.45M	91.44
GeoLoRA	0.47M	98.55	0.35M	91.63
abc-PSI	0.34M	98.57	0.34M	90.93

$A, B \in \mathbb{R}^{n \times r}$ and r is fixed. A and B are updated simultaneously by gradient descent.

2. AdaLoRA [47], which parametrizes $Y = USV^T$, but in contrast to the proposed method, U, S , and V are updated by simultaneous gradient descent. U and V are regularized to be approximately orthogonal and a singular value truncation criterion on S is used to mask or reactivate singular values and the corresponding basis functions.
3. GeoLoRA [40], a recently proposed rank-adaptive method for low-rank training and fine-tuning with convergence and optimality guarantees similar to the proposed method.

We present in Table 3 results for fine-tuning the vit-base-patch16-224 vision transformer, which is pre-trained on the ImageNet-1k-dataset. The pre-trained weights are downloaded from the torch-vision python package. For all methods, we augment the key, query, and value matrices from attention layers as well as the three fully connected layers of each transformer block with a low-rank adapter. The biases of each layer are trainable. Additionally, the classifier is augmented with a low-rank adapter. The classifier layer is low-rank by construction, thus its rank is set to the number of classes.

We fine-tune the vision transformer on Cifar10 and Cifar100. Table 3 shows the accuracies and number of parameters of the resulting models. Hyperparameter configurations used to produce these results are given in Table 4. The proposed abc-PSI achieves validation accuracies comparable to the methods in the literature, however, with significantly fewer parameters. The reported parameters constitute as $\sum_{l=1}^L m_l r_l + n_l r_l + r_l^2$, for L low-rank adapter layers for all methods. We remark that during training, the forward and gradient evaluation of the abc-PSI requires only the K, V or the L, U matrices at a time. Only in the truncation step, the U, S, V matrices are required at the same time. This enables more sophisticated implementation strategies, to reduce the real memory footprint during the K and L step to $\sum_{l=1}^L m_l r_l + n_l r_l$. This is not possible in the rank adaptive literature methods AdaLoRA and GeoLoRA, that require U, S, V and their gradients at all times.

6.3. Discussion. This paper introduces the augmented backward-corrected PSI (abc-PSI) method for robust and rank-adaptive low-rank training of neural networks. The abc-PSI is suitable for neural network compression during training and low-rank fine-tuning of pre-trained models. Compared to existing methods, it achieves competitive validation accuracy while providing greater network compression.

TABLE 4
Hyper-parameter setup for fine-tuning vision transformer with abc-PSI.

Dataset	Learning Rate	Batch Size	# Epochs	τ	inital rank
Cifar10	8×10^{-4}	256	5	0.15	32
Cifar100	1×10^{-3}	256	5	0.1	32

We have demonstrated that the proposed method is robust in the presence of small singular values, effectively reduces the training loss when used with stochastic gradient descent, and fulfills local convergence guarantees.

Acknowledgments. All authors sincerely thank Martin Frank for his invaluable support, guidance, and the insightful discussions that helped shape this work. AW acknowledges the Helmholtz Information and Data Science Academy and the Norwegian Artificial Intelligence Research Consortium for funding her research visit at the Norwegian University of Life Sciences as well as the Norwegian University of Life Sciences for hosting her stay, during which much of this work was conducted.

The authors have used ChatGPT, version v2, to edit and polish written text for spelling, grammar, or general style. All authors have carefully examined, and refined the content, taking complete accountability for the finalized version of this manuscript.

REFERENCES

- [1] L. ALZUBAIDI, J. ZHANG, A. J. HUMAIDI, A. AL-DUJAILI, Y. DUAN, O. AL-SHAMMA, J. SANTAMARÍA, M. A. FADHEL, M. AL-AMIDIE, AND L. FARHAN, *Review of deep learning: concepts, cnn architectures, challenges, applications, future directions*, Journal of big Data, 8 (2021), pp. 1–74.
- [2] M. BACHMAYR, H. EISENMANN, E. KIERI, AND A. USCHMAJEW, *Existence of dynamical low-rank approximations to parabolic problems*, Mathematics of Computation, 90 (2021), pp. 1799–1830.
- [3] B. BAH, H. RAUHUT, U. TERSTIEGE, AND M. WESTDICKENBERG, *Learning deep linear neural networks: Riemannian gradient flows and convergence to global minimizers*, Information and Inference: A Journal of the IMA, 11 (2022), pp. 307–353.
- [4] T. BROWN, B. MANN, N. RYDER, M. SUBBIAH, J. D. KAPLAN, P. DHARIWAL, A. NEELAKANTAN, P. SHYAM, G. SASTRY, A. ASKELL, ET AL., *Language models are few-shot learners*, Advances in neural information processing systems, 33 (2020), pp. 1877–1901.
- [5] G. CERUTI, L. EINKEMMER, J. KUSCH, AND C. LUBICH, *A robust second-order low-rank bug integrator based on the midpoint rule*, BIT Numerical Mathematics, 64 (2024), p. 30.
- [6] G. CERUTI, J. KUSCH, AND C. LUBICH, *A rank-adaptive robust integrator for dynamical low-rank approximation*, BIT Numerical Mathematics, 62 (2022), pp. 1149–1174.
- [7] G. CERUTI, J. KUSCH, AND C. LUBICH, *A parallel rank-adaptive integrator for dynamical low-rank approximation*, SIAM Journal on Scientific Computing, 46 (2024), pp. B205–B228.
- [8] G. CERUTI AND C. LUBICH, *An unconventional robust integrator for dynamical low-rank approximation*, BIT Numerical Mathematics, 62 (2022), pp. 23–44.
- [9] M. COURBARIAUX, I. HUBARA, D. SOUDRY, R. EL-YANIV, AND Y. BENGIO, *Binarized neural networks: Training deep neural networks with weights and activations constrained to +1 or -1*, arXiv:1602.02830, (2016).
- [10] T. A. D’ANTONOLI, L. K. BERGER, A. K. INDRAKANTI, N. VISHWANATHAN, J. WEISS, M. JUNG, Z. BERKARDA, A. RAU, M. REISERT, T. KÜSTNER, ET AL., *Totalsegmentator mri: Sequence-independent segmentation of 59 anatomical structures in mr images*, arXiv preprint arXiv:2405.19492, (2024).
- [11] M. DENIL, B. SHAKIBI, L. DINH, M. RANZATO, AND N. DE FREITAS, *Predicting parameters in deep learning*, Advances in neural information processing systems, 26 (2013).
- [12] L. EINKEMMER, *Accelerating the simulation of kinetic shear alfvén waves with a dynamical low-rank approximation*, Journal of Computational Physics, 501 (2024), p. 112757.
- [13] L. EINKEMMER AND C. LUBICH, *A low-rank projector-splitting integrator for the vlasov–poisson*

- equation, *SIAM Journal on Scientific Computing*, 40 (2018), pp. B1330–B1360.
- [14] J. FRANKLE AND M. CARBIN, *The lottery ticket hypothesis: Finding sparse, trainable neural networks*, arXiv preprint arXiv:1803.03635, (2018).
- [15] Y. GUO, A. YAO, AND Y. CHEN, *Dynamic network surgery for efficient dnns*, *Advances in neural information processing systems*, 29 (2016).
- [16] J. HAEGEMAN, C. LUBICH, I. OSELEDETS, B. VANDEREYCKEN, AND F. VERSTRAETE, *Unifying time evolution and optimization with matrix product states*, *Physical Review B*, 94 (2016), p. 165116.
- [17] B. HASSIBI AND D. STORK, *Second order derivatives for network pruning: Optimal brain surgeon*, *Advances in neural information processing systems*, 5 (1992).
- [18] A. HATAMIZADEH, J. SONG, G. LIU, J. KAUTZ, AND A. VAHDAT, *Diffit: Diffusion vision transformers for image generation*, in *European Conference on Computer Vision*, Springer, 2025, pp. 37–55.
- [19] S. HAYOU, N. GHOSH, AND B. YU, *Lora+: Efficient low rank adaptation of large models*, 2024, <https://arxiv.org/abs/2402.12354>.
- [20] Y. HE, X. ZHANG, AND J. SUN, *Channel pruning for accelerating very deep neural networks*, in *Proceedings of the IEEE international conference on computer vision*, 2017, pp. 1389–1397.
- [21] A. HNATIUK, J. KUSCH, L. KUSCH, N. R. GAUGER, AND A. WALTHER, *Stochastic aspects of dynamical low-rank approximation in the context of machine learning*, TBA, (2024).
- [22] M. HOCHBRUCK, M. NEHER, AND S. SCHRAMMER, *Rank-adaptive dynamical low-rank integrators for first-order and second-order matrix differential equations*, *BIT Numerical Mathematics*, 63 (2023), p. 9.
- [23] E. J. HU, Y. SHEN, P. WALLIS, Z. ALLEN-ZHU, Y. LI, S. WANG, L. WANG, AND W. CHEN, *Lora: Low-rank adaptation of large language models*, arXiv preprint arXiv:2106.09685, (2021), <https://arxiv.org/abs/2106.09685>.
- [24] F. KHADER, G. MÜLLER-FRANZES, S. TAYEBI ARASTEH, T. HAN, C. HAARBURGER, M. SCHULZE-HAGEN, P. SCHAD, S. ENGELHARDT, B. BAESSLER, S. FOERSCH, ET AL., *Denoising diffusion probabilistic models for 3d medical image generation*, *Scientific Reports*, 13 (2023), p. 7303.
- [25] R. KHALITOV, T. YU, L. CHENG, AND Z. YANG, *Chordmixer: A scalable neural attention model for sequences with different length*, in *The Eleventh International Conference on Learning Representations*.
- [26] M. KHODAK, N. TENENHOLTZ, L. MACKEY, AND N. FUSI, *Initialization and regularization of factorized neural layers*, in *International Conference on Learning Representations*, 2021.
- [27] E. KIERI, C. LUBICH, AND H. WALACH, *Discretized dynamical low-rank approximation in the presence of small singular values*, *SIAM Journal on Numerical Analysis*, 54 (2016), pp. 1020–1038.
- [28] E. KIERI AND B. VANDEREYCKEN, *Projection methods for dynamical low-rank approximation of high-dimensional problems*, *Computational Methods in Applied Mathematics*, 19 (2019), pp. 73–92.
- [29] O. KOCH AND C. LUBICH, *Dynamical low-rank approximation*, *SIAM Journal on Matrix Analysis and Applications*, 29 (2007), pp. 434–454.
- [30] J. KUSCH, *Second-order robust parallel integrators for dynamical low-rank approximation*, arXiv preprint arXiv:2403.02834, (2024).
- [31] Y. LECUN, J. DENKER, AND S. SOLLA, *Optimal brain damage*, *Advances in neural information processing systems*, 2 (1989).
- [32] Z. LI, H. LI, AND L. MENG, *Model compression for deep neural networks: A survey*, *Computers*, 12 (2023), p. 60.
- [33] V. LIALIN, N. SHIVAGUNDE, S. MUCKATIRA, AND A. RUMSHISKY, *Relora: High-rank training through low-rank updates*, 2023, <https://arxiv.org/abs/2307.05695>.
- [34] C. LUBICH AND I. V. OSELEDETS, *A projector-splitting integrator for dynamical low-rank approximation*, *BIT Numerical Mathematics*, 54 (2014), pp. 171–188.
- [35] P. MOLCHANOV, S. TYREE, T. KARRAS, T. AILA, AND J. KAUTZ, *Pruning convolutional neural networks for resource efficient inference*, in *International Conference on Learning Representations*, 2017.
- [36] E. H. S. NORSETT AND G. WANNER, *Solving ordinary differential equations i: Nonsti problems*, 1987.
- [37] H. SATO, *Riemannian optimization and its applications*, vol. 670, Springer, 2021.
- [38] S. SCHOTTHÖFER, E. ZANGRANDO, J. KUSCH, G. CERUTI, AND F. TUDISCO, *Low-rank lottery tickets: finding efficient low-rank neural networks via matrix differential equations*, *Advances in Neural Information Processing Systems*, 35 (2022), pp. 20051–20063.
- [39] S. SCHOTTHÖFER AND M. P. LAIU, *Federated dynamical low-rank training with global loss*

- convergence guarantees*, 2024, <https://arxiv.org/abs/2406.17887>.
- [40] S. SCHOTTHÖFER, E. ZANGRANDO, G. CERUTI, F. TUDISCO, AND J. KUSCH, *Geolora: Geometric integration for parameter efficient fine-tuning*, 2024, <https://arxiv.org/abs/2410.18720>.
- [41] M. VALIPOUR, M. REZAGHOLIZADEH, I. KOBYZEV, AND A. GHODSI, *Dylora: Parameter efficient tuning of pre-trained models using dynamic search-free low-rank adaptation*, 2023, <https://arxiv.org/abs/2210.07558>.
- [42] H. WANG, S. AGARWAL, AND D. PAPALIOPOULOS, *Pufferfish: Communication-efficient models at no extra cost*, Proceedings of Machine Learning and Systems, 3 (2021), pp. 365–386.
- [43] T. WEISSMANN, Y. HUANG, S. FISCHER, J. ROESCH, S. MANSOORIAN, H. AYALA GAONA, A.-O. GOSTIAN, M. HECHT, S. LETTMAIER, L. DELOCH, ET AL., *Deep learning for automatic head and neck lymph node level delineation provides expert-level accuracy*, Frontiers in Oncology, 13 (2023), p. 1115258.
- [44] J. WU, C. LENG, Y. WANG, Q. HU, AND J. CHENG, *Quantized convolutional neural networks for mobile devices*, in Proceedings of the IEEE conference on computer vision and pattern recognition, 2016, pp. 4820–4828.
- [45] E. ZANGRANDO, S. SCHOTTHÖFER, G. CERUTI, J. KUSCH, AND F. TUDISCO, *Rank-adaptive spectral pruning of convolutional layers during training*, in Advances in Neural Information Processing Systems, 2024.
- [46] E. ZANGRANDO, S. SCHOTTHÖFER, G. CERUTI, J. KUSCH, AND F. TUDISCO, *Geometry-aware training of factorized layers in tensor tucker format*, 2024, <https://arxiv.org/abs/2305.19059>.
- [47] Q. ZHANG, M. CHEN, A. BUKHARIN, N. KARAMPATZIAKIS, P. HE, Y. CHENG, W. CHEN, AND T. ZHAO, *Adalora: Adaptive budget allocation for parameter-efficient fine-tuning*, 2023, <https://arxiv.org/abs/2303.10512>.
- [48] J. ZHAO, Z. ZHANG, B. CHEN, Z. WANG, A. ANANDKUMAR, AND Y. TIAN, *Galore: Memory-efficient llm training by gradient low-rank projection*, 2024, <https://arxiv.org/abs/2403.03507>.
- [49] X. ZHAO, L. WANG, Y. ZHANG, X. HAN, M. DEVECI, AND M. PARMAR, *A review of convolutional neural networks in computer vision*, Artificial Intelligence Review, 57 (2024), p. 99.

Author contribution statement (CRediT). **Jonas Kusch:** Conceptualization, Methodology, Formal analysis, Writing - Original Draft, Supervision. **Steffen Schotthöfer:** Methodology, Software, Benchmarking, Writing - Original Draft, Supervision. **Alexandra Walter:** Methodology, Formal analysis, Software, Writing - Original Draft, Visualization

Appendix A. Proof of Lemma 5.7. In the following, we restate Lemma 5.2. of [21] for the stochastic gradient.

Proof. We have for a general $Z : \mathbb{R}_+ \rightarrow \mathbb{R}^{m \times n}$

$$\frac{d}{dt}\ell(Z(t)) = \langle \nabla\ell(Z(t)), \dot{Z}(t) \rangle.$$

With the fundamental theorem of calculus,

$$\begin{aligned} \ell(Z_1) &= \ell(Z_2) + \int_0^1 \frac{d}{dt}\ell(Z_2 + t(Z_1 - Z_2))dt \\ (A.1) \quad &= \ell(Z_2) - \int_0^1 \langle \nabla\ell(Z_2 + t(Z_1 - Z_2)), Z_1 - Z_2 \rangle dt. \end{aligned}$$

Then, with zero completion using $\pm\nabla\ell(Z_2)$ and pulling out the of t independent term from the integral, (A.1) becomes

$$\begin{aligned} \ell(Z_1) &= \ell(Z_2) - \langle \nabla\ell(Z_2), Z_1 - Z_2 \rangle \\ &\quad - \int_0^1 \langle \nabla\ell(Z_2 + t(Z_1 - Z_2)) - \nabla\ell(Z_2), Z_1 - Z_2 \rangle dt. \end{aligned}$$

Using the Cauchy-Schwarz inequality and Assumption A2, yields

$$\begin{aligned}
& - \int_0^1 \langle \nabla \ell(Z_2 + t(Z_1 - Z_2)) - \nabla \ell(Z_2), Z_1 - Z_2 \rangle dt \\
& \leq \int_0^1 \|\nabla \ell(Z_2 + t(Z_1 - Z_2)) - \nabla \ell(Z_2)\| \cdot \|Z_1 - Z_2\| dt \\
& = c_l \int_0^1 \|(Z_2 + t(Y - Z_2) - Z_2)\| \cdot \|Z_1 - Z_2\| dt \\
& = c_l \int_0^1 t \|(Z_1 - Z_2)\|^2 dt.
\end{aligned}$$

Hence,

$$\ell(Z_1) \leq \ell(Z_2) - \langle \nabla \ell(Z_2), Z_1 - Z_2 \rangle + \frac{c_l}{2} \|Z_1 - Z_2\|^2,$$

concluding the proof of the Lemma. \square